# Mechanistic understanding of transition between quantized conductance plateaus under strain perturbation

Mark D. Huntington,[1] Jason N. Armstrong,[1] Matthew R. Sullivan,[1] Susan Z. Hua,[1,*] and Harsh Deep Chopra[1,2,*]
[1]*Thin Films & Nanosynthesis Laboratory, State University of New York, Buffalo, New York 14260, USA*
[2]*Division of Materials Research, National Science Foundation, Arlington, Virginia 22230, USA*
(Received 16 December 2007; revised manuscript received 18 May 2008; published 29 July 2008)

The quantum of electronic conductance is $2e^2/h$ ($G_o$) corresponding to a fully open transmission channel. Nonquantized conductance values or transition between conductance plateaus in nonintegral values of $G_o$ are observed when the available channels are partially transmitting or when the system is subjected to a perturbation. Through the development of a simple method based on differential in coefficient of thermal expansion between a metal point contact and the underlying substrate, the present study succeeds in resolving the complete and contiguous mechanistic structure of transition between adjacent conductance plateaus under strain perturbation. Using gold as a model system, results reveal three distinct stages during the controlled extraction of a single atom from a given point contact—two stages where the conductance fluctuates due to partially open channels, separated by an intermediate stage of random telegraphic noise characterizing mechanical instability of the contact. Whereas random telegraphic noise in larger contacts was previously attributed to fluctuations of metastable defects between discrete configurations [K. S. Ralls and R. A. Buhrman, Phys. Rev. Lett. **60**, 2434 (1988); K. S. Ralls and R. A. Buhrman, Phys. Rev. B **44**, 5800 (1991)], its appearance in the present study is attributed to the fluctuations of a metastable contact between discrete configurations having slightly different transmission probabilities. In addition to Au, preliminary studies on Cu and Ni show similar behavior, pointing to the universal nature of the transition. The technique can be easily applied to study multivalent elements, magnetic atoms, as well as molecular electronics and mechanics.

DOI: 10.1103/PhysRevB.78.035442 PACS number(s): 81.07.Lk, 81.16.Ta, 81.07.Vb

## I. INTRODUCTION

Atomic corrals, atomic or molecular wires, molecular devices, and other similarly sized structures are test beds for probing physical properties in the size regime where quantum effects dominate.[1–6] Such atomic-sized structures offer the possibility of tuning physical properties of interest through "design" of electronic structure.[1,7,8] In addition, recent years have seen rapid progress in nanofabrication of templates toward the goal of making reproducible nanostructures; see for example, Ref. 9. These efforts also represent emerging frontiers for pursuing "science beyond Moore's law." The quantum of electronic conductance is $2e^2/h$ ($\equiv 1G_o = 7.748091 \times 10^{-5}$ siemens or $1/12906\ \Omega^{-1}$; $e$ is the electron charge, $h$ is Planck constant).[10,11] This was first demonstrated in mesoscale constrictions in a two-dimensional electron gas (2DEG).[12,13] Nonquantized conductance values or transitions between conductance plateaus in fractional values of $G_o$ occur when the available channels are partially transmitting,[14] or when the system is subjected to a perturbation (electric field,[15–18] magnetic field,[19–22] strain,[23] etc.). While mesoscale 2DEG systems are ideal for various perturbation studies, they are less amenable to strain. In the present study, we have developed a simple method that succeeds in resolving the mechanistic structure of transitions between adjacent conductance plateaus under strain perturbation, using metal point contacts. Results reveal three distinct stages associated with the removal of a single atom from a contact of a given diameter, and link them directly to the observed fine features of the conductance histogram. Characteristic examples of fluctuations of metastable contacts between discrete configurations are also discussed.

The technique developed in the present study utilizes the differential in coefficient of thermal contraction between a substrate and a short (micrometer or less), narrow (few atoms in diameter) metal bridge joining two mechanically constrained microfabricated electrodes; no moving mechanical parts or piezodrivers are needed. By varying the temperature, we find that the differential in coefficient of thermal contraction between the bridge and the substrate provides a high degree of control to precisely vary the bridge diameter, and with ease. Advantage is taken of the fact that there is a large differential in coefficient of thermal contraction between silicon ($2.6 \times 10^{-6}\ K^{-1}$; silicon being the material of choice in microfabrication) and most common metals (for example, Na: 71; Au: 14.2; Ag: 18.9; Co: 13; Ni: 13.4; Cu: 15.5; Pt: 8.8; in units of $10^{-6}\ K^{-1}$). This differential causes stress to build up at the metal nanoconstriction (the metal bridge) whereby it becomes possible to controllably reduce its diameter atom-by-atom by a small change in temperature. This change can be continuously monitored by measurement of conductance across the bridge.

## II. EXPERIMENTAL DETAILS

Figure 1(a) shows scanning electron micrograph (SEM) of microfabricated gold electrodes, which are subsequently joined together by an electrodeposited bridge of predetermined diameter. Special microfabrication steps were taken to ensure that the electrodes are mechanically constrained to the substrate. To accomplish this, photolithography was used to form 50–100 nm deep channels, 50 $\mu$m wide, on a silicon wafer by reactive ion etching. Then a Ta (7.5 nm) seed layer was deposited inside the channels on which 300 nm thick Au

 

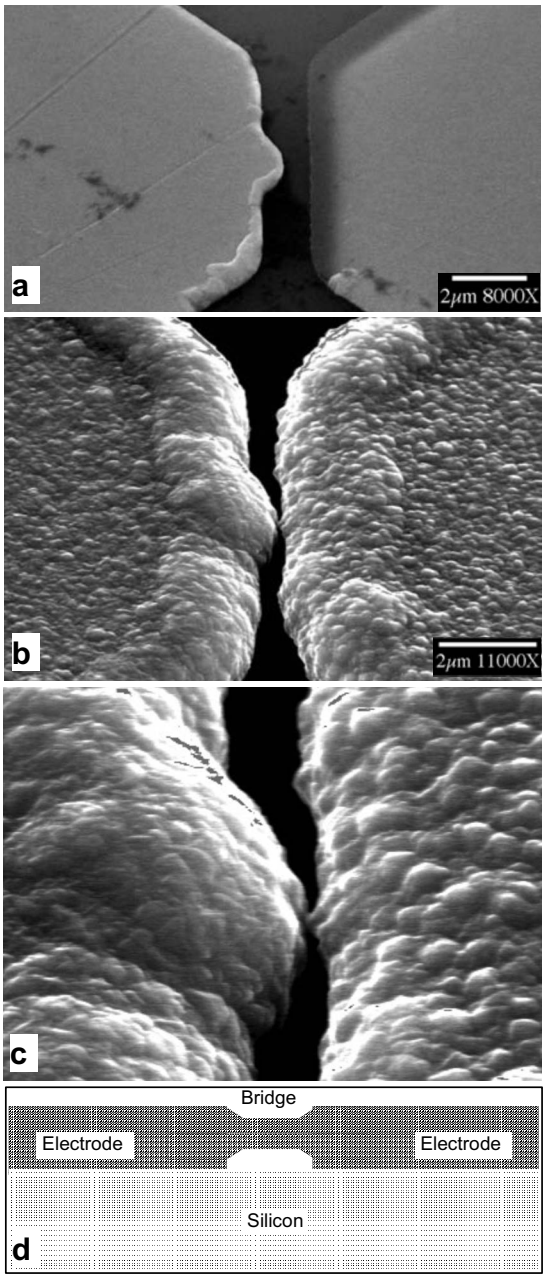


FIG. 1. (a) Scanning electron micrograph of microfabricated gold electrodes. Sputter-deposited gold electrodes were further thickened by electrodeposition to ≈2 $\mu$m prior to the formation of a point contact between them. (b) SEM of a gold point contact across the electrodes. For the purpose of imaging, a larger diameter contact (~20 nm) is shown, whereas in actual experiments, the contact was typically 4–10 atoms in diameter. (c) A magnified view of the contact shown in (b). (d) Schematic showing a point contact between electrodes that are mechanically constrained by the underlying silicon substrate. A layer of silicon oxide (not shown) is also present between the electrodes and the silicon substrate in actual devices.

film was sputter deposited, Fig. 1(a). The gap between the electrodes in Fig. 1(a) is ≈0.75 $\mu$m; smaller gaps can be readily made using focused ion beam. The sputter-deposited gold electrodes were then thickened to ≈2 $\mu$m by electrodeposition using a noncyanide electrolyte (Techni-Gold 25 from Technic Inc.); solution pH 6.5–7.5; current density 14.8 mA/cm$^2$. This was followed by electrodeposition of a narrow gold bridge across the electrodes, Fig. 1(b), using the self-termination method.[24] The self-termination electrodeposition method enables a bridge of any predetermined diameter to be readily made to a size resolution of a single atom (4–10 atoms in diameter in the present study). The electrodeposited bridge was formed by placing a drop of supersaturated KCl solution on the electrodes at an applied voltage of 1.4 V, with the microfabricated tip serving as cathode and the opposite lead as anode. Figure 1(c) shows a magnified view of the electrodeposited bridge. The schematic in Fig. 1(d) shows a mechanically unconstrained bridge that is free to contract (expand) on cooling (heating) across mechanically constrained thin-film electrodes. An electrodeposited bridge ensures a metallic bond across the electrodes prior to stretching it in a cryogenic chamber with inert helium atmosphere. Prior to the transfer of the chip into the cryogenic chamber, the bridged electrodes were thoroughly rinsed and dried by continuously flushing the electrolyte in de-ionized ultrafiltered water, followed by drying with nitrogen gas. Note that while bridges 4–10 atoms in diameter may appear fragile, they were found to be sufficiently robust to survive their transfer into the cryogenic chamber. The cryogenic chamber is capable of heating or cooling the sample in an inert He atmosphere from 1.9 to 350 K with an accuracy of 0.01 K [Physical Property Measurement System (PPMS) from Quantum Design]. In addition to Au, preliminary experiments were also conducted on Cu and Ni. Nickel bridges across Ni electrodes were electrodeposited using nickel sulfamate solution (84 g/l Ni as metal in $Ni(SO_3NH_2)_2.2H_2O$; 30 g/l boric acid, pH 3.3) at an applied voltage of 1.0 V.[25] Copper bridges across Cu electrodes were formed using supersaturated KCl solution, at an applied voltage of 1.0 V.

Initially, our efforts were focused on assessing the efficacy of the technique. This often caused an overshoot in the temperature during cooling/heating the samples in trying to controllably break the contacts. However, we did not encounter problems with repeated use of the samples. In fact, to avoid taking the data from the same sample, different samples were used. In the overall process, the critical step is the electrodeposition of the initial bridge that is small but robust enough to withstand cleaning/drying followed by its insertion in the cryogenic chamber. If an electrodeposited contact has a large diameter, it may not break down to the last atom even after cooling it to 1.9 K. On the other hand, if the contact diameter is too small, it can break during the cleaning/transfer process. Repeated electrodeposition to obtain a stable contact of optimum diameter can ultimately cause the microfabricated tip to blunt, and such samples have to be discarded. In our procedure, we optimized the initial Au contact size to ≈4–10 atoms.

A source meter (Keithley 2400) was used as the voltage source and current monitor for conductance experiments. The source voltage was maintained through a servo system that is internal to the instrument. On top of the servo system a compliance circuit was used to maintain the compliance limits of the source. This ensures that the instrument can

maintain a constant voltage. For these experiments the instrument was configured to function in the normal output "off" state. In this state the source voltage is set to zero and the current compliance is set to 5% of the full range compliance. This "soft off" state provides relatively high impedance off state while preventing the system from experiencing any type of shock that could disturb the atomic system while turning the source on or off. The voltage source is connected to the sample and an external resistor, which are wired in series. Voltage measurements are taken over the external resistor. The constant resistance of the external resistor ensures that at all times the impedance of the acquisition system is much higher than that of the input so that the measurement has negligible effect on the overall circuit. The conversion factor between the measured voltage and conductance is $G/G_o=[V_m/(V_o-V_m)](12\,906/R_{\text{ext}})$, where $V_m$ is the measured voltage on the external resistor $R_{\text{ext}}$, in series with the point contact, $V_o$ is the total supplied voltage, and $G/G_o$ is the conductance in units of $G_o(=1/12\,906\ \Omega^{-1})$. Unless otherwise noted, the external resistor $R_{\text{ext}}$ was always kept at 25 812 $\Omega$ $(G_o/2=1/25\,812\ \Omega^{-1})$; $V_o$ was 1.4 V for Au, and 1.0 V for Ni and Cu. The data acquisition was done using a National Instruments PCI-6036E series data-acquisition card with 16 bit resolution and 100 G$\Omega$ input impedance. The negative terminal of the voltage source was connected to the analog ground plane of the card. All cables were also shielded and grounded to further reduce noise. To build the conductance histogram, 243 complete traces were used; in addition, several hundred (~700) additional traces, where the contact broke abruptly after obtaining only a partial section of the complete transition, were also included in the histogram. All the measured traces were fed into the computer for automated binning. The conductance histogram was built by binning the measured voltages in sections of 100 mV. The counts per bin were plotted versus bin voltage in units of $G_o$ using the above conversion factor. To quantify the amplitude of conductance fluctuations, statistical analysis was done on these same traces to calculate the average and standard deviation. For each trace, the average of the measured voltage was calculated. Also, the standard deviation was calculated using the relationship $\text{var}=\frac{1}{n-1}\Sigma_{i=1}^{n}(X_i-\bar{X})^2$; standard deviation $=\sqrt{\text{var}}$. Here, $\bar{X}$ is the average and $n$ is the length of that section (~2000 points/section). The results were binned in sections of $0.1G_o$. For each bin, the average was plotted versus the corresponding $G_o$ value. The variance of points within each bin was used to determine the error bars [in Fig. 8(b)].

## III. RESULTS AND DISCUSSION

The prototypical metal system of gold was chosen for the present study. The malleable and inert nature of gold allows ease of formation of point contacts that exhibit reproducible conductance behavior even when made under different conditions.[26,27] For monovalent gold, each atom provides a single mode for conductance. Therefore, for gold the number of available channels can be tuned simply by adding or subtracting an atom, as shown in inset-I of Fig. 2. Note that rather than studying the characteristics of conductance plateaus, the focus of the present study was to gain a mechanistic understanding of the stepwise transition (marked by dotted lines in inset-I of Fig. 2) under strain perturbation. Of course this first requires ability to make stable contacts. Figure 2 shows three conductance traces from stable contacts ranging in diameter from 1 to 3 atoms, made by the differential thermal contraction technique. While Fig. 2 shows 10 min of recorded traces (owning to large data files), contacts could be held stable for hours. Several contacts could even be held stable for a period of over 24 h and in one instance a contact could be stabilized for over 54 h. Inset-II of Fig. 2 highlights the characteristics of conductance traces near integral (≈1, 2, and 3 $G_o$) and nonintegral values (~1.5 and 2.5 $G_o$). When a metal bridge is being progressively reduced in diameter from three, to two, to one atom, large fluctuations appear in the measured signal at nonintegral conductance values due to partially open transmission channels, as shown in inset-II. A mechanistic understanding of precisely how such transitions occur is the focus of the present study.

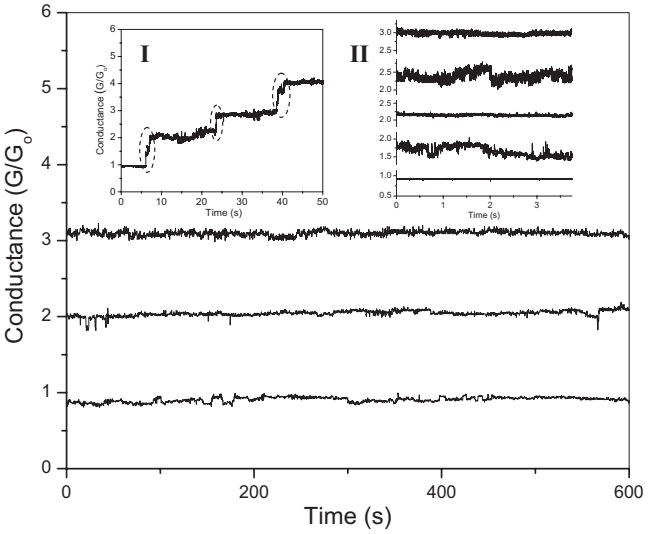


FIG. 2. Conductance traces across stable one-, two-, and three-atom gold point contacts. The traces at nominal values of 1, 2, and 3 $G_o$ were measured after stabilizing the respective contacts at 263, 244.5, and 270.5 K using the present technique. *Inset-I:* Addition of a single gold atom causes a stepwise increase in conductance from one plateau to the next. This trace was obtained by electrodeposition of gold at room temperature by self-termination method (Ref. 24). The structure of the steps (highlighted by dotted lines) under strain perturbation is the focus of the present study. *Inset-II:* Using the present technique, as the diameter of a gold contact is reduced by stretching, large conductance fluctuations appear at nonintegral values (≈1.5 and ≈2.5 $G_o$). In contrast, note the minimal conductance fluctuations across stable contacts at ~1, 2, and 3 $G_o$.

Figure 3(a) shows a typical conductance trace illustrating the mechanistic sequence associated with reducing the diameter of the contact by a single atom. The trace in Fig. 3(a) reveals three distinct stages (marked consecutively as "$\alpha$," "$\beta$," and "$\gamma$") during the transition from a stable two-atom contact (region labeled "$X$") to a stable single-atom contact (region labeled "$Y$"). Note that the trace in Fig. 3(a) reveals the structure of the "step" connecting two adjacent quantized conductance plateaus *under strain perturbation*. Beginning

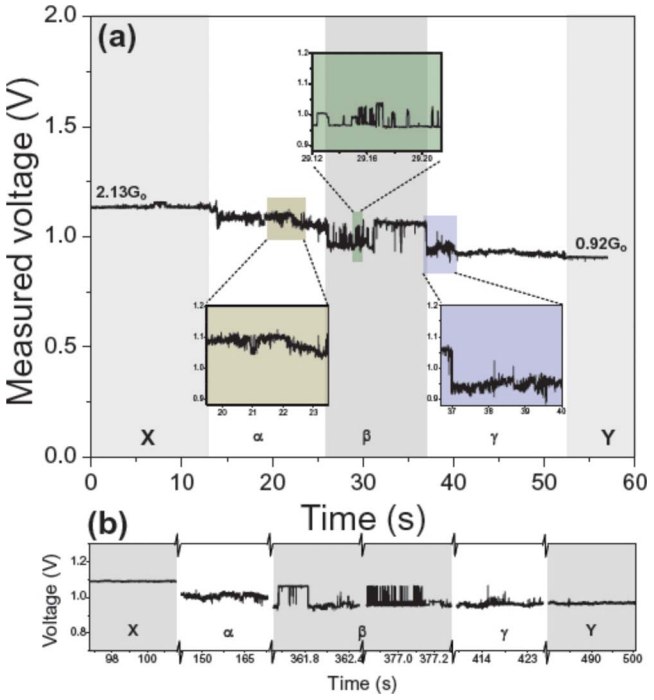


FIG. 3. (Color online) (a) Conductance trace during the controlled extraction of a single atom from a two-atom Au contact at ~242 K. Stages X and Y correspond to a stable two-atom and a stable single-atom contact, respectively. The transition from 2 to 1 $G_o$ occurs in three consecutive stages, denoted by $\alpha$, $\beta$, and $\gamma$. Insets show magnified views of small sections of the trace within each stage. (b) The consecutive conductance trace using the same sample as in (a) highlighting the repeatability of the observed transition sequence. The trace in (b) was measured at ~241 K. For clarity, only truncated sections of the trace are shown due to its long duration.

with the two-atom conductance plateau, as the contact is slowly stretched, the interatomic distances increase, diminishing the transmission probabilities for available channels. This causes the conductance to fluctuate (between ≈1.3 to 2.2 $G_o$ in this example) and this range is labeled $\alpha$ in Fig. 3(a). A magnified view of a section of the conductance trace in this region is shown as an inset. In comparison, note the marked suppression of conductance fluctuations in the measured signal corresponding to maxima in transmission probability for the two-atom (region *X*) and single-atom contacts (region *Y*). Further stretching leads to mechanical instability in the contact, and this region is labeled $\beta$ in Fig. 3(a). In this region, the metastable contact fluctuates between discrete configurations, leading to the appearance of stepwise or random telegraphic noise in the measured signal. The maximum amplitude of random telegraphic noise roughly lies between the values of conductance in stages *X* and *Y*. A magnified view of the random telegraphic noise in this region is shown as an inset. The kinetics and characteristics of random telegraphic noise as a consequence of fluctuations of metastable contact between discrete geometric configurations are discussed later. With further stretching, the single-atom configuration ultimately becomes relatively more stable than the two-atom configuration, and this stage is labeled $\gamma$ in Fig. 3(a). Analogous to stage $\alpha$, this region is characterized by conductance fluctuations (≈0.85–1.2 $G_o$) due to imperfect transmission across the last available channel of a single-atom contact. A magnified view of a section of the trace in this region is shown in the inset. Finally, the contact relaxes into a stable single-atom configuration with a marked suppression of conductance fluctuations in the measured signal corresponding to maxima in transmission probability. Thus the overall mechanistic structure of the transition consists of stages $\alpha$ and $\gamma$ where the channels are partially open, and stage $\beta$ where the contact shows mechanical instability. Nonquantized transitions are well documented in 2DEG constrictions,[15–18] even though the underlying mechanism there is different. Nonetheless, in both cases, nonquantized transitions occur as a result of a device-specific perturbation.

In terms of precision and accuracy of the measurements to repeated temperature cycles, the differential thermal straining technique provides reasonable precision (to within a fraction of a degree Kelvin) in terms of stabilizing a contact at a given temperature, and moderate accuracy (1–3 K) in breaking it again at the same temperature. For example, once a given contact is completely broken apart, reforming and stabilizing it requires heating the sample by up to 10° above the temperature it broke. Following this, it again breaks within ≈3 K of the original temperature. We attribute this variation to the relative change in position and distance between the nearest atoms across the tips, requiring slightly different temperatures to re-form the contacts. While no two traces are ever alike in the details of their time-dependent behavior (nor expected), they follow the same transition sequence as described in Fig. 3(a). To illustrate, Fig. 3(b) shows the consecutive conductance trace from the same sample as in Fig. 3(a). It highlights the repeatability of the observed transition sequence and at high time-resolution.

In addition to detailed studies on Au, preliminary studies on Ni and Cu reveal a similar transition behavior. This universality of the observed behavior under strain perturbation is highlighted for different sized contacts in Figs. 4(a) and 4(b) for Ni and Cu, respectively. Note that due to the relatively low ductility of Ni in comparison to Au, some telegraphic noise is also present in stages $\alpha$ and $\gamma$, resulting in a slight overlap of different stages. The observed behavior is also technique independent. Using a slowly approaching (1 nm/s) Au tip toward a sputter-deposited gold substrate in a home-made STM at room temperature, qualitatively similar characteristics were found. The well defined transition sequences in Fig. 3 or Figs. 4(a) and 4(b) are to be contrasted with the behavior of an uncontrollably breaking contact, where different conductance stages were found to completely overlap one another. This is shown in Fig. 4(c) for the case of an unstable Ni contact at room temperature soon after it was electrodeposited. In this instance, the contact began to break before it could be successfully transferred into the cryogenic chamber. The two magnified insets in Fig. 4(c) show random telegraphic noise due to the mechanical instability of the contact riding on the undulating signal from partially open channels.

The present technique also provides the ability to study time-dependent behavior over extended periods of time in any given region of the transition. This is highlighted in Fig. 5(a) for a gold contact in the region of mechanical instability,

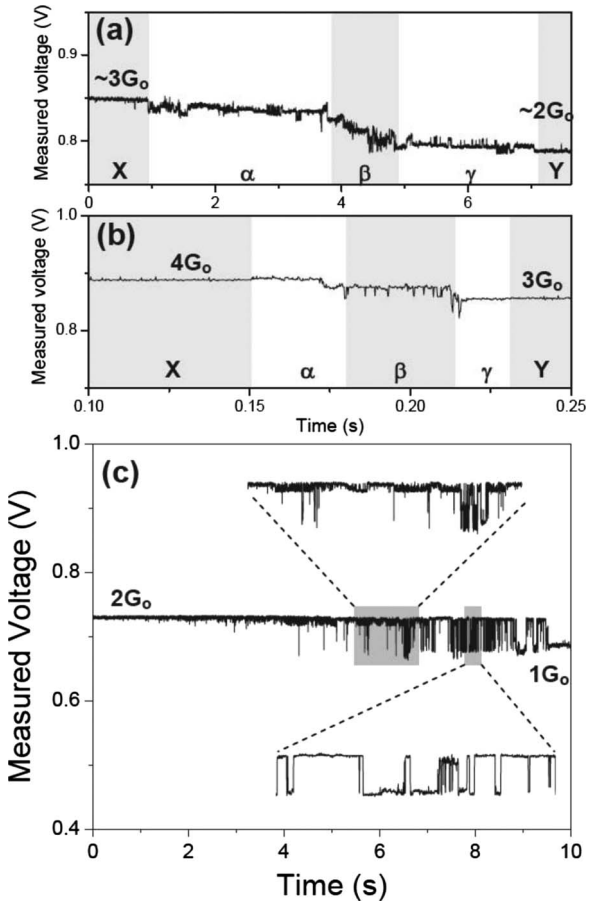


FIG. 4. Conductance traces during the controlled extraction of a single atom from different sized point contacts in different systems using the present technique. (a) Ni from 3 to 2 $G_o$ at ~288 K. (b) Cu from 4 to 3 $G_o$ at ~280 K. (c) A conductance trace from an uncontrollably breaking Ni contact at room temperature, which causes different transition regions to overlap one other.

as it transitions from a two-atom to a single-atom contact. A closer examination of the trace in Fig. 5(a) reveals that the entire trace is comprised of random telegraphic noise, as shown in the magnified views of different sections along the trace. Random telegraphic noise has previously been observed in various devices.[15–18,28–31] In particular, earlier work on larger diameter metal nanocontacts (where quantized conductance is not dominant) by Ralls and Buhrman[28] provides a potentially fruitful "analysis template" for interpreting telegraphic noise in these quantum conductors. In case of Ralls and Buhrman, the telegraphic noise was attributed to the fluctuation of metastable defects between discrete configurations. In the present study, strain perturbation causes metastable contact geometry to fluctuate between discrete configurations leading to slightly different transmission probabilities, and manifesting as random telegraphic noise.

Several illustrative examples of telegraphic noise are shown in Figs. 5(b), 5(c), 6, and 7 (which also parallel various examples shown in Ralls and Buhrman, but with a different interpretation). Figure 5(b) shows a two-level fluctuation, along with a schematic (red curve); the low conductance state is labeled as 1 and the high conductance state is labeled as 2. A histogram of time durations in either the low or the high conductance states was found to be exponential, and the observed telegraphic noise follows the Markov model—the system's memory is no longer than the last state occupied. Using a two-state Markov model shown in Fig. 5(b), the mean time it takes to transition from configuration state 1 to configuration state 2 is 1.23 ms, and the mean time to transition from $2 \rightarrow 1$ is 1.25 ms. However, note that the actual data are more complex than can be accurately modeled by the simple two-state model shown in Fig. 5(b) since the Markov chain can be seen to exhibit multiple open/closed states (as evident from multiple bursts in the chain) that become activated/inactivated in time; a more rigorous analysis is beyond the scope of the present study and will be reported in the future. Also note that while the attempt frequency to go from state $1 \rightarrow 2$ may be very high (of the order of atomic vibrations), the observed switching rates may be much lower, as seen from the two-state model. However, without further studies (currently in progress), we cannot yet extract the pre-exponential term, and can only measure the relative rates.

Very often, a high-frequency two-level telegraphic noise is seen riding on a low frequency two-level telegraphic noise, an example of which is shown in Fig. 5(c). In the schematic shown in Fig. 5(c), the low-frequency train is shown in red, on which the high-frequency (green) train is riding. This indicates a higher energy barrier for the low-frequency jumps, and a lower energy barrier for the high-frequency jumps. Whereas the low-frequency noise may arise from fluctuations between discrete metastable contact configurations with a high energy barrier between them, the high-frequency jumps are likely related to additional (rotational, etc.) degrees of freedom within a given metastable configuration. In the present study, the prevalent cases involve change in frequency or/and the amplitude of the high-frequency telegraphic noise as the slowly reconfiguring contact geometry fluctuates between its high and low conductance states. Whereas, examples of amplitude modulation were found to be rare in Refs. 28, such examples abound in the case of quantum conductors. Two such examples are shown in Figs. 6(a) and 6(b). For the example shown in Fig. 6(a), it can be seen that the amplitude of the high-frequency telegraphic noise is higher (an overall larger change in the net transmission probability) when it rides the high conductance state of the slowly reconfiguring contact geometry. Two-state Markov models for the rapidly configuring contact geometry on successive high and low conductance states of the slowly reconfiguring contact geometry reveal an interesting behavior. Figure 6(a) shows that the mean time it takes to transition from configuration state 1 (or $1'$) to configuration state 2 (or $2'$) remains virtually unchanged (from 3.34 to 3.33 to 4.85 ms). In contrast, the mean time it takes to transition from configuration state 2 (or $2'$) to configuration state 1 (or $1'$) varies by an order of magnitude (from 67.9 to 6.9 to 17.0 ms). In other words, the stationarity (variations in mean time for transitions over extended periods) is nearly zero in going from $1 \rightarrow 2$ (or $1' \rightarrow 2'$) and highly variable for transitions occurring from $2 \rightarrow 1$ (or $2' \rightarrow 1'$). A large stationarity (in either direction) is indicative of a rapidly reconfiguring contact. The transition of the system toward an overall more stable configuration is better

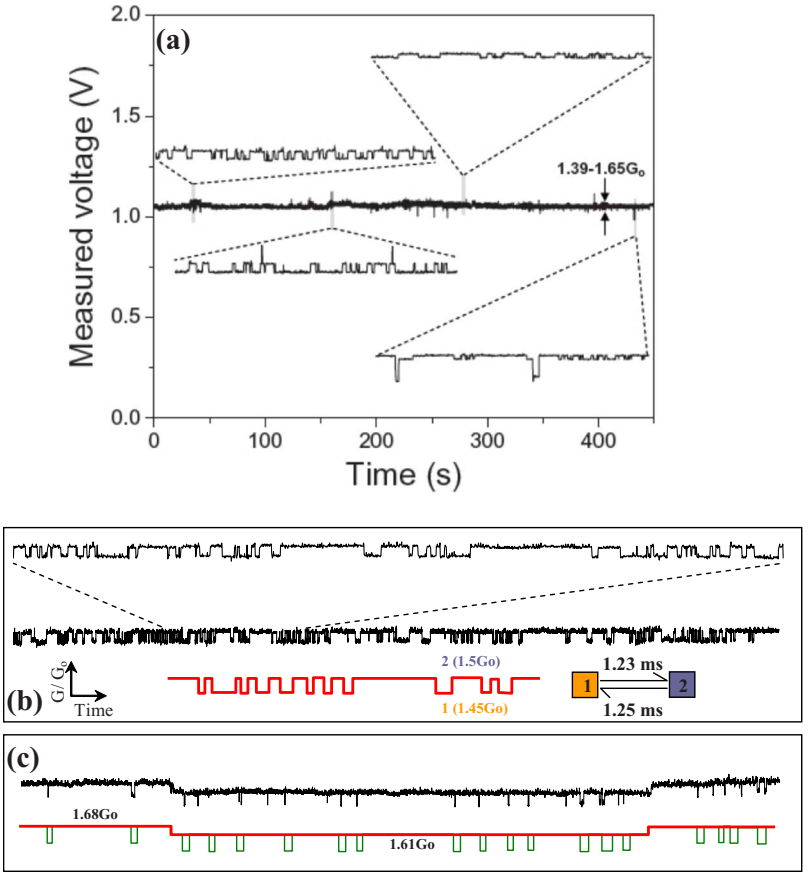


FIG. 5. (Color online) (a) A long-duration conductance trace of a gold point contact in the region of mechanical instability as it transitions from a two-atom to a single-atom contact. Zoomed views show various profiles of random telegraphic noise at different sections along the trace. The trace was measured at ~243 K. (b)–(c) Illustrative examples of random telegraphic noise in gold point contacts in the region of mechanical instability at ~243 K. (b) A two-level random telegraphic noise train along with a schematic (red curve). The two-state Markov model shows an approximately equal mean time to transition from state $1 \rightarrow 2$ (1.23 ms) and from state $2 \rightarrow 1$ (1.25 ms) over the entire length of the Markov chain. (c) A metastable contact that slowly configures between two discrete conductance states (shown in red in the schematic) over which a high-frequency telegraphic noise (shown in green in the schematic) is riding.

illustrated with the help of the example shown in Fig. 6(b). The interesting feature of this example is that throughout the measured signal, the transmission probability of state 2 for the high-frequency noise riding on the low conductance state of the slowly reconfiguring contact geometry is equal to the transmission probability of state $1'$ riding on the high conductance state of the slowly reconfiguring contact geometry. The magnified view in Fig. 6(b) and the schematic also emphasizes the observation that the transition always occurred from state 1 to state $2'$ (and vice versa) and never from state 1 to $1'$ (or between $1'$ and 2). In other words, the slowly reconfiguring contact attempts to reach the same state (state 2 or equivalently state $1'$) from its low and high conductance state, respectively. Over time, the system eventually achieves this state, as shown in the truncated trace in Fig. 6(c), which illustrates the collapse of the slowly configuring contact geometry into a new two-state metastable configuration.

Figure 7(a) shows an example of frequency modulation. In Fig. 7(a), transition between the two discrete levels is seen to occur at two different frequencies—a low-frequency fluctuation (shown in red in the schematic) and a higher frequency fluctuation (shown in green in the schematic). Such a Markov chain is best modeled as having three states belonging to two distinct classes; in this example, the class with lower conductance has two states labeled 1 and $1'$, whereas the class with high conductance has a single state labeled 2 in Fig. 7(a). The resulting three-state model is also shown in Fig. 7(a). The model shows that the mean time it takes to transition between the low-frequency states 1 and 2 is approximately the same (48.84 and 51.17 ms, respectively). In contrast, when the system is in state 2, it can transition back and forth between 2 and $1'$ at higher frequency; the mean times from $2 \rightarrow 1'$ being 9.65 ms and that from $1' \rightarrow 2$ being 0.99 ms. Figure 7(b) shows an example where the contact configuration fluctuates between three discrete states. A closer examination of these fluctuations reveals that the fluctuations always occur between states $1 \leftrightarrow 2$ or between $2 \leftrightarrow 3$ (except for the solitary initial jump to an intermediate state at the beginning of the Markov chain); the corresponding three-state Markov model with mean times for transitions between various states is also shown in Fig. 7(b). This example illustrates the existence of two energy barriers of comparable height that are available relative to state 2, and across which the system fluctuates either between $1 \leftrightarrow 2$ or $2 \leftrightarrow 3$.

To summarize, it is emphasized that the observed transition sequences in Figs. 3 or 4 describe the behavior of a contact under strain perturbation as a single atom is being controllably extracted from it. Whereas the universality of the transition sequence is illustrated by observation of similar behavior in different metallic systems (Au, Cu, and Ni), its repeatability was confirmed by consistently observing the same transition sequence over a large number of traces, using Au (243 complete traces and several hundred additional partial traces where the contact broke abruptly). The conductance histogram over all the traces is shown in Fig. 8(a); various peaks (green) in the histogram were fitted with Gaussian distribution (blue). As a comparison, the conductance histogram for the single trace shown in Fig. 3(a) is also included as an inset in Fig. 8(a). The variations in the amplitude of conductance fluctuations versus contact diameter (in

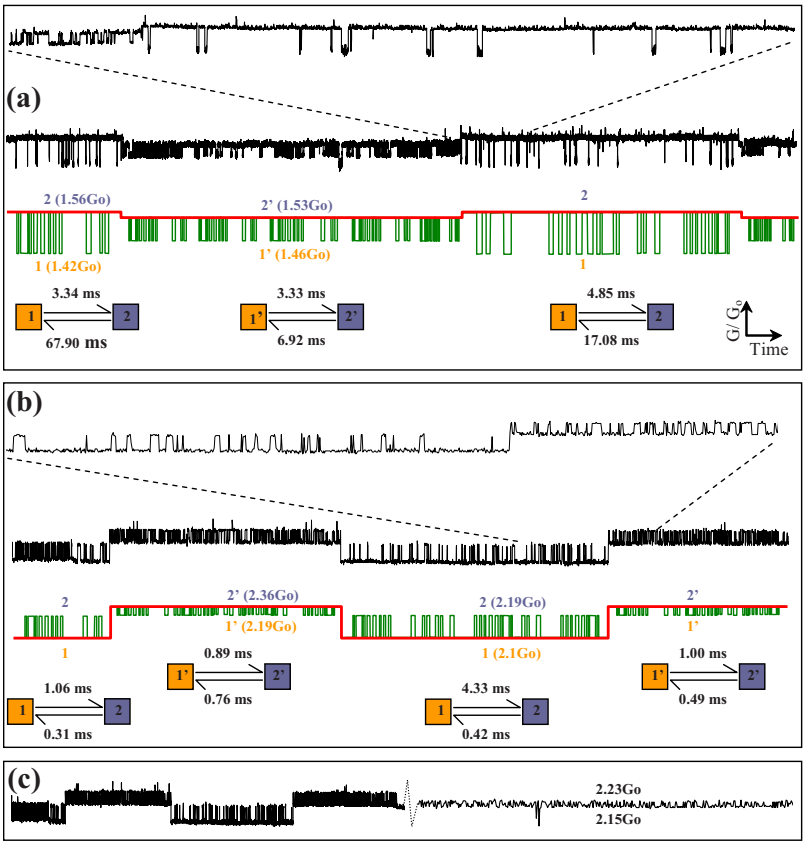


FIG. 6. (Color online) Examples of amplitude modulation in mechanically unstable contacts, along with schematics of the telegraphic noise. Various two-state Markov models correspond to high-frequency telegraphic noise (shown as green in the schematics) for each segment (high and low conductance states) of the low-frequency noise (shown as red in the schematics). (a) The Markov models for different sections of the trace obtained from a Au contact at ~243 K reveal a large variation in mean time to transition from $2 \rightarrow 1$. In contrast, the mean time to transition from $1 \rightarrow 2$ remains essentially unchanged. (b) Example of amplitude modulation in a Ni point contact at 266 K and 1 T. (c) Same Ni contact as in (b), which eventually collapses into a new two-state metastable configuration. See text for explanation.

terms of $G_o$) is statistically summarized for the entire set of measured traces (complete and partial) in Fig. 8(b). Confirming the visible traits of the observed conductance traces such as those shown in Figs. 3 and 4, Fig. 8(b) shows a marked suppression in amplitude of conductance fluctuations at ~0.9, 2.1, and 3 $G_o$, corresponding to the maxima in transmission probabilities in stable contacts; the observed behavior is also in qualitative agreement with previous studies[32–34]

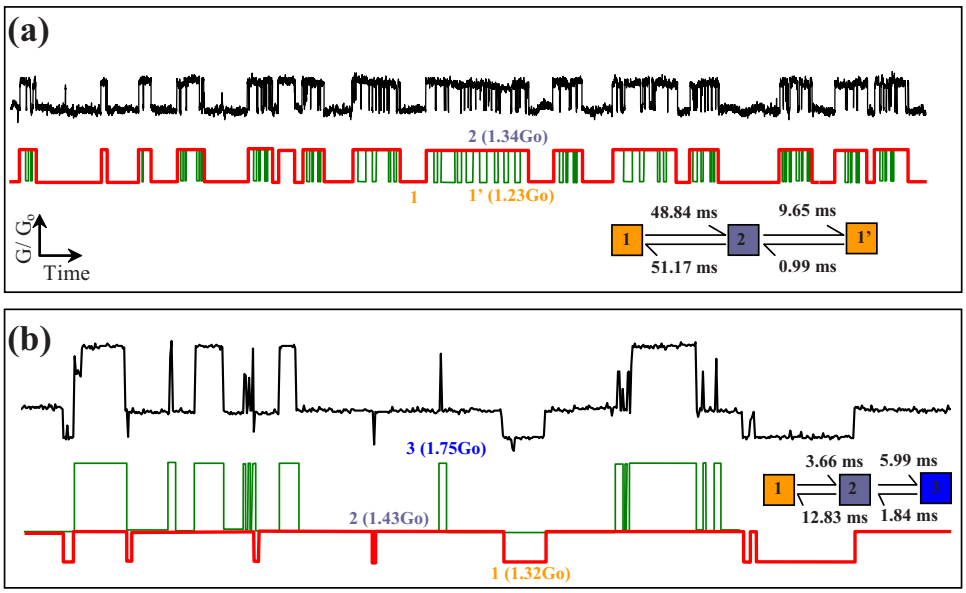


FIG. 7. (Color online) (a) Example of frequency modulation in a mechanically unstable Au contact at ~243 K, along with a schematic. This Markov chain is best modeled as a two-class (I and II) system, with class "I" having two states (labeled 1, 1′) and class "II" having a single state (labeled 2). The two different states (1 and 1′) within class I are represented by the same color (orange) in the Markov model. (b) An example of a mechanically unstable Au contact at ~243 K, along with a schematic. In this Markov chain, the contact configuration fluctuates between two different states (1 and 3) relative to state 2. This example is best modeled as having three classes (I, II, and III), with each class having a single state (labeled 1, 2, and 3, respectively).

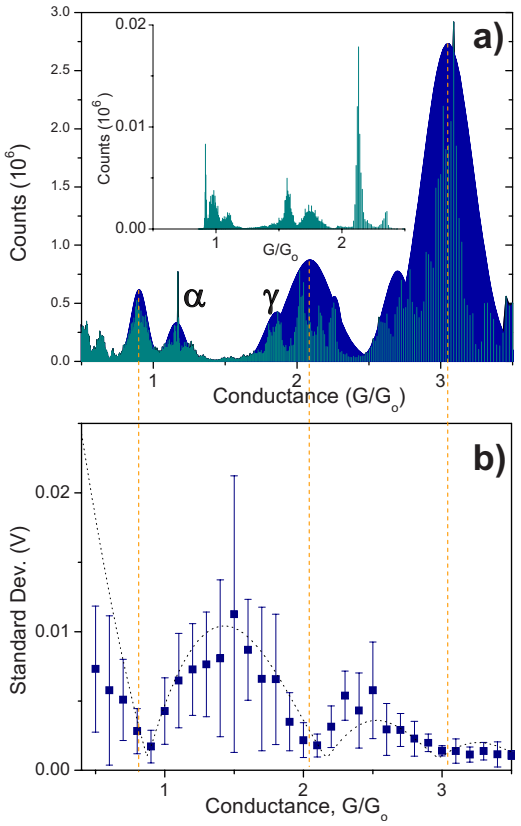


FIG. 8. (Color online) (a) The measured conductance histogram for Au at ~242 K. This histogram was built using 243 traces. In addition, several hundred partial traces (~700) where contact broke abruptly are also included in this histogram. Inset shows the histogram of the single trace shown in Fig. 3(a). The blue peaks are Guassian fits to the measured (green) peaks. (b) Variation in amplitude of conductance fluctuation as a function of contact diameter (in terms of $G_o$) at ~242 K. The plot was built using the same 243 traces and ~700 partial traces where contact broke abruptly. As shown by the (orange) dotted guide lines, minima in amplitude of conductance fluctuations occur at ~0.9, 2.1, and 3 $G_o$, which correspond to histogram peaks for stable one-, two-, and three-atom contacts in (a). See Sec. II for further experimental details regarding (a) and (b).

and highlights the robustness of the present technique. The minima in Fig. 8(b) match well with the corresponding peaks for stable contacts in the conductance histogram, as shown by the dotted (orange) lines running from Figs. 8(a) and 8(b). Additionally, in Fig. 8(a) peaks labeled $\alpha$ and $\gamma$ correspond to stages $\alpha$ and $\gamma$ shown in the conductance traces in Fig. 3. *Note that the statistical analysis is well suited to describe the position of the quantized values. However, it is not designed to capture the time-resolved transient behavior shown in Figs. 3–7, such as the two level fluctuations.*

## IV. CONCLUSIONS

To conclude, a simple and straightforward technique based on differential coefficient of thermal contraction has been developed to study quantum point contacts under strain perturbation; no movable mechanical parts or piezodrivers are needed. The method offers the ability to controllably extract a single atom from a given point contact, enabling mechanistic study of transition structure between adjacent conductance plateaus. The transition involves two stages where conductance fluctuates due to partially open channels. These stages are separated by an intermediate stage characterizing mechanical instability of the contact. The mechanical instability manifests as random telegraphic noise arising from fluctuations of a metastable contact between discrete configurations having slightly different transmission probabilities. The universality of the observed transition sequence is illustrated using three different metallic systems. The technique can be easily applied to study more complex ferromagnetic atoms where spin-split states are expected, molecular electronics, mechanics of molecules, and thermally activated processes such as thermal fluctuations of spins states across magnetic atoms, or thermally assisted domain-wall fluctuations.

## ACKNOWLEDGMENTS

M.D.H and J.N.A. contributed equally to this work. Work supported by NSF-DMR-FRG-0305242 and NSF-DMR-0706074, and this support is gratefully acknowledged. Microfabrication was performed, in part, at the Cornell Nanofabrication Facility, which is supported by the NSF Grant ECS-9731293, Cornell University, and industrial affiliates. Any opinions, findings, and conclusions or recommendations expressed in this publication are those of the author(s) and do not necessarily reflect the views of the National Science Foundation. Correspondence and request for materials should be addressed to H.DC. or S.Z.H.

*Corresponding authors: hchopra@eng.buffalo.edu or zhua@eng.buffalo.edu

†

[1] M. F. Crommie, C. P. Lutz, and D. M. Eigler, Science **262**, 218 (1993).
[2] A. Yazdani, D. M. Eigler, and N. D. Lang, Science **272**, 1921 (1996).
[3] C. Joachim, J. K. Gimzewski, and A. Aviram, Nature (London) **408**, 541 (2000).
[4] J. K. Gimzewski and R. Möller, Phys. Rev. B **36**, 1284 (1987).
[5] S. Frank, P. Poncharal, Z. L. Wang, and W. A. de Heer, Science **280**, 1744 (1998).
[6] L. Venkataraman, Y. S. Hong, and P. Kim, Phys. Rev. Lett. **96**, 076601 (2006).
[7] E. J. Heller, M. F. Crommie, C. P. Lutz, and D. M. Eigler, Nature (London) **369**, 464 (1994).
[8] N. Nilius, T. M. Wallis, and W. Ho, Science **297**, 1853 (2002).
[9] D. E. Johnston, D. R. Strachan, and A. T. C. Johnson, Nano Lett.

**7**, 2774 (2007).
[10] R. Landauer, IBM J. Res. Dev. **1**, 223 (1957).
[11] M. Büttiker, Y. Imry, R. Landauer, and S. Pinhas, Phys. Rev. B **31**, 6207 (1985).
[12] D. A. Wharam, M. Pepper, H. Ahmed, J. E. F. Frost, D. G. Hasko, D. C. Peacock, D. A. Ritchie, and G. A. C. Jones, J. Phys. C **21**, L887 (1988).
[13] B. J. van Wees, H. van Houten, C. W. J. Beenakker, J. G. Williamson, L. P. Kouwenhoven, D. van der Marel, and C. T. Foxon, Phys. Rev. Lett. **60**, 848 (1988).
[14] E. Scheer, P. Joyez, D. Esteve, C. Urbina, and M. H. Devoret, Phys. Rev. Lett. **78**, 3535 (1997).
[15] G. Timp, R. E. Behringer, and J. E. Cunningham, Phys. Rev. B **42**, 9259 (1990).
[16] D. H. Cobden, N. K. Patel, M. Pepper, D. A. Ritchie, J. E. F. Frost, and G. A. C. Jones, Phys. Rev. B **44**, 1938 (1991).
[17] C. Dekker, A. J. Scholten, F. Liefrink, R. Eppenga, H. van Houten, and C. T. Foxon, Phys. Rev. Lett. **66**, 2148 (1991).
[18] D. H. Cobden, A. Savchenko, M. Pepper, N. K. Patel, D. A. Ritchie, J. E. F. Frost, and G. A. C. Jones, Phys. Rev. Lett. **69**, 502 (1992).
[19] H. van Houten, C. W. J. Beenakker, P. H. M. van Loosdrecht, T. J. Thornton, H. Ahmed, M. Pepper, C. T. Foxon, and J. J. Harris, Phys. Rev. B **37**, 8534 (1988).
[20] B. R. Snell, P. H. Beton, P. C. Main, A. Neves, J. R. Owers-Bradley, L. Eaves, O. Henini, O. H. Hughes, S. P. Beaumont, and C. D. W. Wilkinson, J. Phys.: Condens. Matter **1**, 7499 (1989).
[21] J. B. Miller, I. P. Radu, D. M. Zumbühl, E. M. Levenson-Falk, M. A. Kastner, C. M. Marcus, L. M. Pfeiffer, and K. W. West, Nat. Phys. **3**, 561 (2007).
[22] H. D. Chopra, M. R. Sullivan, J. N. Armstrong, and S. Z. Hua, Nat. Mater. **4**, 832 (2005).
[23] M. Okamoto and K. Takayanagi, Phys. Rev. B **60**, 7808 (1999).
[24] S. Boussaad and N. J. Tao, Appl. Phys. Lett. **80**, 2398 (2002).
[25] M. R. Sullivan, D. A. Boehm, D. A. Ateya, S. Z. Hua, and H. D. Chopra, Phys. Rev. B **71**, 024412 (2005).
[26] M. Brandbyge, J. Schiøtz, M. R. Sørensen, P. Stoltze, K. W. Jacobsen, J. K. Nørskov, L. Olesen, E. Laegsgaard, I. Stensgaard, and F. Besenbacher, Phys. Rev. B **52**, 8499 (1995).
[27] Z. Gai, Y. He, H. Yu, and W. S. Yang, Phys. Rev. B **53**, 1042 (1996).
[28] K. S. Ralls and R. A. Buhrman, Phys. Rev. Lett. **60**, 2434 (1988); K. S. Ralls and R. A. Buhrman, Phys. Rev. B **44**, 5800 (1991).
[29] R. T. Wakai and D. J. Van Harlingen, Phys. Rev. Lett. **58**, 1687 (1987).
[30] R. T. Wakai and D. J. van Harlingen, Appl. Phys. Lett. **49**, 593 (1986).
[31] F. Liu, M. Bao, K. L. Wang, D. Zhang, and C. Zhou, Phys. Rev. B **74**, 035438 (2006).
[32] Y. P. Li, D. C. Tsui, J. J. Heremans, J. A. Simmons, and G. W. Weimann, Appl. Phys. Lett. **57**, 774 (1990).
[33] F. Liefrink, J. I. Dijkhuis, and H. van Houten, Semicond. Sci. Technol. **9**, 2178 (1994).
[34] H. E. van den Brom and J. M. van Ruitenbeek, Phys. Rev. Lett. **82**, 1526 (1999).